Synthesis and *In Vitro* Biological Evaluation of a Second-Generation Multimodal Water-Soluble Porphyrin-RAPTA Conjugate for the Dual-Therapy of Cancers

*Jordon Sandland,[a] Huguette Savoie,[a] Ross W. Boyle,[*a] and Benjamin S. Murray.[*a]*

a Department of Chemistry and Biochemistry, University of Hull, Cottingham Road, Hull, E. Yorkshire, HU6 7RX, UK. E-mail: r.w.boyle@hull.ac.uk, b.s.murray@hull.ac.uk.

KEYWORDS

porphyrin • RAPTA • dual-therapy • photosensitiser • theranostic.

ABSTRACT

In this study we report the synthesis and biological evaluation of a novel cationic porphyrin-[Ru(η^6-arene)(C_2O_4)PTA] (RAPTA) conjugate with potential as a multimodal dual-therapeutic agent. In the absence of high intensity light, relative to untreated cells our conjugate resulted in a 83% decrease in viable human adenocarcinoma cells at a concentration of 10 μM, which is significantly more active than the 57% decrease achieved with the same concentration of the unconjugated RAPTA complex alone. With a light dose of 20 J cm^{-2} (400 – 1200 nm) a reduction

of 98% of viable cells was observed for the same concentration of conjugate. The conjugate is internalized by HT-29 cancer cells as proven by ICP-MS analysis and fluorescence microscopy: the latter result suggesting that the conjugate has applications as a multimodal agent by acting as a fluorophore to obtain *in vivo* biodistribution data. Furthermore, the conjugate has an excellent relative singlet oxygen quantum yield, and the tetrapyrollic unit was found to be photostable under irradiation by either white light or red light.

INTRODUCTION

Increasingly, novel metal-based compounds are being investigated as cytotoxic agents. Of key significance in this area are ruthenium-based organometallic compounds of which the ruthenium(II) arene 1,3,5-triaza-7-phosphaadamantane (PTA) family, or so-called "RAPTA" complexes, have gained interest in the past two decades as anti-angiogenic or anti-metastatic agents.[1,2] The distinct, but promiscuous, biomacromolecular interactions of many ruthenium-based compounds offers promise in overcoming limitations associated with traditional platinum-based and organic-based chemotherapeutics.[3,4] For example, platinum-based therapies are associated with more than 40 side effects[5] and many cancers become resistant to platinum *via* mechanisms including: decline in adduct levels, reaction with intracellular reducing agents, binding to transporters, reduced endocytosis and cross-linking repair.[6] The unique chemistry of many ruthenium-based metallodrugs may enable these issues to be circumvented. Like clinically approved platinum-based chemotherapeutics, the majority of ruthenium-based metallodrugs operate via mechanisms of action dominated by the aquation of the metal center followed by metalation of intra- or extracellular biomacromolecular targets.[7] However, the elucidation of the *in vivo* biodistribution of ruthenium-based metallodrugs, such as the RAPTA family, is challenging

and has only been achieved via invasive biopsies followed by elemental analysis such as ICP-MS techniques or by analyzing the radioactivity of resected organs (when a ^{103}Ru-labelled compound was utilized).[8]

Porphyrins are well known for their fluorescent properties, and also an ability to generate cytotoxic reactive oxygen species (ROS) by energy or electron transfer from the excited triplet state, upon interaction with light.[9] Porphyrins have previously been used to generate theranostic agents for combined cancer therapy and imaging.[10] Photodynamic therapy (PDT) is a minimally invasive technique requiring a photosensitizer (PS), light and molecular oxygen. Absorption of light of the correct wavelength promotes the porphyrin into an electronically excited singlet state which undergoes Laporte forbidden intersystem crossing to the triplet state.[11] From there, two main photochemical processes can occur to produce cytotoxic species. The Type I mechanism creates ROS through immediate electron transfer to surrounding substrates, while the Type II mechanism is dominated by interaction with molecular oxygen producing singlet oxygen.[11] An added and well documented, yet controversial,[12] benefit of conjugating to porphyrins is they are able to utilize the enhanced permeation and retention (EPR) effect to passively accumulate and be retained in tumors, this has been proven with many substrates appended to porphyrins which has been demonstrated in both murine models and humans.[13,14,15]

It is well understood that cancers are far less resilient when combating two therapies at the same time, and, the combination of PDT with the anti-metastatic/cytotoxic effects of a ruthenium(II) metallodrug represents an underexplored therapeutic combination. While the conjugation of

porphyrins with pyridyl groups to Ru-(η^6-arene) complexes has been carried out previously, four ruthenium moieties were required to obtain IC_{50} values in the low micro molar region.[16] A different study investigated the photophysical properties of first generation ruthenium-porphyrin conjugates using 2,2'-bipyridine groups on the porphyrin macrocycle to act as ligands to the metal center.[17] Cytotoxicity was observed in the low micromolar range albeit with four ruthenium metal centers appended to the porphyrin. There is clear scope to improve the activity of such conjugates with a concomitant reduction in the number of appended Ru-(η^6-arene) groups. Furthermore, these Ru-(η^6-arene)-porphyrin conjugates possessed limited aqueous solubility as a result of the highly lipophilic porphyrin components and lipophilic bifunctional linkers, highlighted by the use of organic solvent to acquire spectral data for these compounds.[16]

Clearly, further development of Ru-(η^6-arene)-porphyrin conjugates is required in order to produce a clinically relevant and economically viable chemotherapeutic possessing a single metal center that is sufficiently hydrophilic. The employment of hydrophilic porphyrins bearing solubilizing methyl pyridinium groups and a hydrophilic bifunctional spacer is obviously advantageous. Furthermore, cationic N-methylpyridyl porphyrins possess a natural ability to passively accumulate in cancer cells and neoplastic tissues.[18] It has been well documented elsewhere that cationic N-methylpyridinium porphyrins are internalized by cancer cells, often localizing to the mitochondria,[19,20] and lysosomes.[21,22] Therefore, our studies have focused on a cationic porphyrin covalently tethered to a single [Ru(η^6-arene)(C_2O_4)PTA] complex with an established reactivity profile.

As previously discussed, several attempts to synthesise tetranuclear Ru(II)-porphyrin conjugates have been reported, however, in these previous examples the ruthenium ion was coordinated to the porphyrin via N-heterocycle nitrogen atoms. We have investigated the tethering of the [Ru(η^6-arene)(C_2O_4)PTA] complex by the arene ring, thus enabling the known reactivity of the ruthenium complex to be unimpeded by its conjugation to the porphyrin. As discussed, the mechanism of action of these [Ru(η^6-arene)(C_2O_4)PTA] complexes is exerted through coordination of biomacromolecular targets to the metal centre in the extra- and intracellular environment.

EXPERIMENTAL

General information

All reagents were reagent grade and purchased from Fluorochem, Alfa Aesar, and Sigma Aldrich and were used as received, unless stated otherwise. Dry solvents were obtained by drying over activated 4Å or 3Å molecular sieves or anhydrous metal salts as stated for at least 24 h. Bulk solvents were removed at an appropriate temperature using a Buchi rotavapor R-210 at reduced pressure with a Vacuubrand PC101 membrane pump. Solids were dried overnight or until reaching constant mass in a vacuum oven (Buchi glass oven B-585) at 40 ºC. Reaction progress and purity were analysed by TLC using Fluka analytical TLC plates (0.2 mm thickness and 10 cm length; silica 60 Å). TLC was visualized using UV irradiation. (Spectroline; ENF-260C/FBE). Products were purified by column chromatography using an appropriate mobile phase as stated using a glass chromatography column and a stationary phase of silica gel obtained from Fluorochem; LC60Å 35-70 μm. Progress of column chromatography was visualized using UV irradiation, tracked against relevant TLC plates. NMR were recorded on a JEOL ECZ 400 spectrometer at 400 MHz

for proton NMR and at 100.5 MHz for carbon NMR. All samples contained an internal standard of tetramethylsilane (TMS) in deuterated solvent as stated. NMR spectra splitting patterns were designated as s (singlet), d (doublet), m (multiplet) or br s (broad singlet), dd (doublet of doublets) as appropriate. All chemicals shifts, δ, for proton and carbon NMR spectra were quoted as parts per million, ppm. J values are quoted in Hz unless stated otherwise. Mass spectrometry data was obtained by the EPSRC National Mass Spectrometry Service at Swansea. Combustion elemental analysis was performed with 15 mg of compound analysed in a Carlo Erba EA1108 CHN Fischer instrument with a thermal conductivity detector for determination of CHN; analysis quoted in %. HPLC analyses were carried out on an Agilent series 1200 HPLC system. Separations were carried out on an ACE-5 C-18 column (4.6 mm x 250 mm). All solvents were HPLC grade containing 0.1% trifluoroacetic acid (TFA) in both eluents. Analytical RP-HPLC (ACE-5, C-18 column, 4.6 mm x 250 mm) with HPLC grade methanol with 0.1% TFA and HPLC grade water with 0.1% TFA as eluents A and B respectively. The flow rate was 1 mL per minute. Initially, an isocratic gradient of 5% rising to 95% (20 mins, isocratic 95% (3 mins), falling to 5% (2 mins) and remaining isocratic 5% A (5 mins). UV-Vis data were obtained from a Varian Cary Bio50 spectrometer with aliquots of standard solutions of known concentration in an optical glass cuvette (path length = 1 cm) of optical clarity 300-900 nm. Data was obtained from solutions of 20 μL additions to 2 mL of solvent from a 10 mL stock solution of concentration $1x10^{-2}$ mol dm^{-3}. The molar extinction coefficient was calculated at the λ max of the Soret band (400-450 nm) by the application of the Beer – Lambert law. Fluorescence data were obtained from a Varian Cary Eclipse spectrometer with aliquots of standard solutions of known concentration in an optical glass cuvette (path length = 1 cm) of optical clarity 300-900 nm. Data was obtained from solutions of

20 μL additions to 2 mL of solvent from a 10 mL stock solution of concentration $1x10^{-2}$ mol dm^{-3}.

Relative singlet oxygen quantum yield

Photo-oxidation experiments were carried out in a quartz fluorescence cuvette (46 x 12.5 x 12.5 mm), aqueous ABDA (2 mL, 150 μM) was added followed by photosensitizer (50 μL, 150 μM). The cuvette was irradiated at 298 K under continuous irradiation from a 600 mW Paterson Xenon short arc lamp equipped with a band pass filter (617-651 nm). The intensity of the light from the same distance was measured with a Macam R203 Radiometer (1035.8 W m^{-2}). Measurements were taken every 10 minutes with a Varian Cary Bio 50 UV-Vis photospectrometer. Experiments were carried out in triplicate (n=3).

Photostability

Porphyrin photostability experiments were carried out in a quartz fluorescence cuvette (46 x 12.5 x 12.5 mm), H_2O (2 mL) was added followed by photosensitizer (100 μL, 150 μM). The cuvette was irradiated at 298 K under continuous irradiation from a 600 mW Paterson Xenon short arc lamp equipped with a band pass filter (617 - 651 nm). The intensity of the light from the same distance was measured with a Macam R203 Radiometer (1035.8 W m^{-2}). Measurements were taken every 60 seconds with a Varian Cary Bio 50 UV-Vis photospectrometer. Experiments were carried out in triplicate (n=3). RAPTA conjugate photostability experiments were carried out in standard NMR tubes by irradiating samples (5 mg) in D2O (0.7 ml). The NMR tube was irradiated at 298 K under continuous irradiation from an Oriel 1000W QTH white light source (400-1200 nm) in 20 J cm^{-2} increments followed by $^{31}P\{^{1}H\}$ NMR analysis.

Cell culture

Human colorectal adenocarcinoma (HT-29) cells were cultured in an incubator with a humidified 5% CO_2 atmosphere at 37 ºC in T25 flasks until reaching 60-75% confluence. RPMI complete media (Life Science Productions) substituted with 1% L-glutamine and 5% foetal bovine serum (Life Science Productions) was used as culture media.

MTT cell viability assay

The cell viability was determined using MTT (3-[4, 5-dimethylthiazol-2-yl]-2, 5 diphenyltetrazolium bromide) colorimetric assay. Briefly: HT-29 cells were seeded onto 96-well plates in complete RPMI media and allowed to attach overnight. Aliquots of compound were administered in complete media and the plates incubated as required. The plates were irradiated using an Oriel 1000W QTH white light source (20 J cm^{-2}). MTT solution (10 μL, 12 mM) is added to each well and incubated for 4 h at 37 °C to allow MTT to be metabolised. The crystals formed were dissolved by adding acid-alcohol mixture (150 μL, 0.04 M HCl in absolute 2-propanol) (Honeywell; puris >99.7% GC). The absorbance at 570 nm was measured on a Biotek ELX800 Universal Microplate Reader (BioTek®, Winooski, VT, USA). The results are expressed with respect to control values (i.e. cells only).

Brightfield/fluorescence imaging

HT-29 cells (10 x 10^3 cells/mL) in McCoy's 5A modified medium substituted with 1% L-glutamine and 10% foetal calf serum (Life Science Productions) were seeded in 35 mm glass dishes and left to attach overnight. The media was discarded and 10 μM of **8** or **9** added and left to incubate at 37 ºC for 24 h. The media was discarded and replaced with PBS thrice. Live-cell

microscopy was carried out using a Leica DM IRB microscope with a Cairn mercury arc lamp, the cut-off filter used was 610 nm.

ICP-MS

HT-29 human adenocolorectal cancer cells (1 mL, 3 x 10^5 cells/mL), with a confluence of 60-70%, were aliquoted into centrifuge tubes (Falcon). The cells were pelleted by centrifugation and re-suspended in 1 mL of McCoy's 5A modified medium substituted with 1% L-gluamine and 10% foetal calf serum (Life Science Productions) or McCoy's 5A modified medium substituted with 1% L-gluamine and 10% foetal calf serum (Life Science Productions) substituted with 10 μM of compounds **2** or **9**. The tubes were incubated for 72 h at 37ºC with a 5% CO_2 humidified environment. The cells were pelleted and the supernatant collected. The cell pellet was re-suspended with PBS (1 mL, Glibco®; PBS tablets) pelleted and the supernatants fractions combined. The pellets and supernatant were frozen at -20ºC for 24 h before ICP-MS processing. The samples were diluted into concentrated nitric acid and water (Elga Purelab Flex). ICP-MS was carried out using an Agilent 7500cx instrument. The cool gas was argon (BOC Cryospeed) with a flow rate of 15 L/min, the auxiliary flow rate was 0.2 L/mins and the nebuliser was 0.8 L/min. The detector (Perkin Elmer) was peltier cooled to -43 ºC. The nebuliser used was a high solids modified V-groove PEEK unit (Perkin Elmer). The Ru standards used were certified 1000 ppm (Romil, UK), which were diluted with 2% v/v nitric acid (Spa grade, Romil, UK) and water (Purelab).

HPLC

HPLC analyses were performed on an Agilent series 1200 HLC system. Separations were carried out on an ACE-5 C-18 column (4.6 x 250 mm). Semi-preparative HPLC was carried out using a

Pursuit 10 μm C-18 200 Å column (250 x 10 mm) (Phenomenex). All solvents were HPLC grade containing 0.1% TFA in both eluents. Analytical RP-HPLC (ACE-5, C18 column, 4.6 x 250 mm 100) with HPLC grade methanol with 0.1% TFA and HPLC grade water with 0.1% TFA as eluents A and B respectively. The flow rate was 1 mL per minute. Initially, an isocratic gradient of 5% A rising to 95% (20 mins), isocratic 95% (3 mins), falling to 5% (2 mins) and remaining isocratic 5% A (5 mins).

Statistical analysis

All biological experiments were carried out in triplicate. All data are given as the mean values, error bars are presented as standard deviations (X±SD) of three independent plated experiments performed in triplicate (n=3). Data were plotted on GraphPad Prism 7.0 using recommended post-hoc statistical testing.

Complex 2 MS analysis

Accurate mass measurements were performed at the University of Hull using a Bruker Maxis Impact QqTOF MSMS. Before mass measurement the instrument was calibrated against sodium formate over the range 90 to 1550 Da. Resolution used was typically 45000. Samples (as solutions in methanol, 10^{-5} M) were injected into a solvent stream from a syringe pump at 3 μl min^{-1} via a 5 μl loop injector. The data was then internally mass measured against an internal calibrant peak from hexakis(1H,1H,4H-hexafluorobutyloxy)phosphazine (CAS No. 186406-47-2) $C_{24}H_{18}O_6N_3P_3F_{36}$ *m/z* 1220.99064. An average result from 3-5 separate injections is quoted. The mass was measured and calculated using Bruker DataAnalysis 4.2 software.

Complex **1** was synthesised as described in Murray, B. S.; Menin, L.; Scopelliti, R.; Dyson, P. J. Conformational control of anticancer activity: the application of arene-linked dinuclear ruthenium(II) organometallics. *Chem. Sci.*, **2014**, *5*, 2536-2545.

Porphyrins **3**-**5** were synthesised according to the method previously described in Yap, Y. Y.; Price, T. W.; Savoie, H.; Boyle R. W.; Stasiuk, G. J. Selective radiolabelling with ^{68}Ga under mild conditions: a route towards a porphyrin PET/PDT theranostic agent. *Chem. Commun.*, **2018**, *54*, 7952–7954.

Complex 2: 2-(1H-Benzotriazole-1-yl)-1,1,3,3-tetramethylaminium tetrafluoroborate (TBTU) (160 mg, 0.498 mmol) and **1** (178 mg, 0.349 mmol) were suspended in DMSO (4 mL) then N,N-diisopropylethylamine (DIPEA) (364 μL, 2.09 mmol) was added and the mixture was left to stir for 5 min. Methylamine hydrochloride (24 mg, 0.355 mmol) was then added and the reaction mixture was left to stir. After 2 h the yellow solution that had formed was added to a silica gel column (4 cm x 20 cm loaded in acetone) with acetone (20 mL) in excess in the solvent reservoir. The solvent was eluted to allow the yellow suspension to settle onto the silica gel. The column was then eluted with acetone (200 mL to remove DMSO) then MeOH (300 mL) followed by MeOH/H_2O (500 ml, 9:1). The product eluted as a yellow solution – this was filtered then dried at 65 °C under reduced pressure. The residue was dissolved in MeOH (30 mL) with heating, allowed to cool and left to vapour diffuse (48 h) with diethyl ether to yield a precipitate. The solvent was decanted and the precipitated solid washed with diethyl ether then dissolved in H_2O (5 mL) and lyophilized to leave the product as an orange solid (51 mg, 0.096 mmol, 28 % (yield based on partially hydrated complex)). ^{1}H NMR (400 MHz, D_2O, 25^{o}C): δ=5.94 (d, J = 6.5 Hz,

2H; Ar-H), 5.90 (d, J = 6.0 Hz, 2H; Ar-H), 4.56 (s, 6H; PTA), 4.15 (s, 6H; PTA), 2.66 (s, 3H; -$NHCH_3$), 2.58 (s, 4H; CH_2-CH_2), 2.05 (s, 3H; Ar-CH_3); $^{31}P\{^1H\}$ NMR (162 MHz, D_2O, 25ºC): δ =-32.8 (s, PTA); $^{13}C\{^1H\}$ NMR (100 MHz, D_2O, 25ºC): δ=174.5, 166.1, 98.8, 96.6, 88.4 (d, J = 3.0 Hz), 87.7 (d, J = 3.5 Hz), 70.7 (d, J = 6.5 Hz), 48.5 (d, J = 15.5 Hz), 35.5, 28.2, 25.8, 17.3; HRMS (ESI^+) m/z $[M+H]^+$ calcd for $C_{19}H_{28}N_4O_5RuP$: 525.0853, found 525.0840; elemental analysis calcd for $C_{19}H_{27}N_4O_5PRu•0.5H_2O$: C 42.86, H 5.30, N 10.52, found: C 42.56, H 5.16, N 10.30.

5-[4-(2-(2-(2-Boc-aminoethoxy)ethoxy)ethaneaminocarbonyl)phenyl]-10,15,20-tris-(4-pyridyl)porphyrin (3):[23] Under an inert atmosphere, to a solution of 5-[4-carboxyphenyl]-10,15,20-tri-(4-pyridyl)porphyrin (500 mg, 755.5 mmol) in DMF (20 mL) was added tert-butyl (2-(2-(2-aminoethoxy)ethoxy)ethyl)carbamate (280 mg, 1.133 mmol) and TBTU (600 mg, 1.133 mmol) and DIPEA (2 mL). The reaction was stirred at 80 ºC overnight. Bulk solvent was removed under reduced pressure. The crude was taken in DCM and washed with copious amounts of water. The organic layer was separated and dried with anhydrous $MgSO_4$. The semi-crude was dissolved in a minimum of DCM and eluted onto a silica chromatography column. The product eluted in DCM/MeOH (93:7) as the first major red band. The fractions were collected and bulk solvent removed under reduced pressure. The solids were dissolved in a minimum of MeOH and precipitated over Et_2O to yield a deep purple crystalline powder (556 mg, 623.0 mmol, 82% yield). R_F: 0.50 (silica, 9:1, DCM/MeOH); ^1H NMR (400 MHz, $CDCl_3$, 25ºC, TMS): δ=9.05 (dd, J=4.4 Hz, 10H; o-Py-H, overlapping 4H; β-H), 8.85 (d, 4H; o-Ar-H, m-Ar-H), 8.16 (dd, J=4.4 Hz, 10H; o-Py-H, overlapping 4H; β-H), 3.73 (m, 12H; CH_2-CH_2), 1.24 (s, 9H; NHBoc), -2.92 (s, 2H, N-H); $^{13}C\{^1H\}$ NMR (100 MHz, $CDCl_3$, 25ºC, TMS): δ=156.08 (C=O), 150.95 (NHBoc), 147.90,

142.90, 134.70, 134.42, 129.66, 128.45, 126.88, 126.70, 125.72, 124.49, 124.45, 118.93, 118.54, 117.45, 110.30, 70.62, 70.37, 55.12, 45.31, 43.21, 40.41, 28.46; HRMS (MALDI) m/z $M^{+\cdot}$ calcd for $C_{53}H_{49}N_9O_5$: 891.3868 found: 891.3851; UV-Vis (DCM): λ_{max} 418 (24742), 516 (3936), 550 (,383), 590 (1678), 651 nm (58 $mol^{-1}dm^3cm^{-1}$).

5-[4-(2-(2-(2-Boc-aminoethoxy)ethoxy)ethaneaminocarbonyl)phenyl]-10,15,20-tris-(N-methyl-4-pyridinium)porphyrin triiodide (4):[23] Under an inert atmosphere, **3** (200 mg, 0.224 mmol) was dissolved in DMF (80 mL) and the flask fitted with a triethylamine trap bubbler. Methyl iodide (3 mL) was added dropwise and the reaction stirred at 40 ºC overnight. Excess diethyl ether (200 mL) as added to the flask and the precipitate filtered off under gravity through a plug of cotton wool. The crude precipitate was dissolved in methanol and precipitated from diethyl ether (100 mL). The product was filtered under reduced pressure to give a burgundy solid which was washed copiously with diethyl ether. The powder was dissolved in a minimum of methanol and precipitated over diethyl ether to give lustrous purple crystals (250 mg, 0.190 mmol, 84% yield). R_F: 0.37 (silica, 8:1:1, acetonitrile/water/$KNO_{3(aq)}$); Rt: 9.75 mins (C-18 silica); ^1H NMR (400 MHz, DMSO-d6, 25ºC): δ=9.44 (d, 6H; m-Py-H), 9.14 (m, 8H; β-H), 8.97 (d, 6H; o-Py-H), 8.31 (d, 2H; m-Ar-H), 7.91 (d, 2H; o-Ar-H), 6.90 (s, 1H; NHBoc), 4.60 (m, 9H; Py-CH_3), 3.14 (m, 4H; CH_2-CH_2), 1.32 (s, 9H; NHBoc), -3.08 (s, 2H; NH); $^{13}C\{^1H\}$ NMR (100 MHz, DMSO-d6, 25ºC): δ=173.99 (C=O), 168.68 (CO-O), 166.68, 164.01, 163.56, 144.64, 137.15, 136.18, 135.39, 130.84, 128.65, 126.95, 125.54, 92.21, 91.49, 80.14, 79.72, 30.29, 23.84; HRMS (ESI+) m/z $[M-3I]^{3+}$ calcd for $C_{56}H_{58}N_9O_5$: 312.1507 found: 312.1515. UV-Vis (MeOH): λ_{max} 426 (91,213), 519 (6601), 560 (2390), 595 (2202), 650 nm (497 $mol^{-1}dm^3cm^{-1}$).

5-[4-(2-(2-(2-Aminoethoxy)ethoxy)ethaneaminocarbonyl)phenyl]-10,15,20-tris-(N-methyl-4-pyridinium)porphyrin triiodide (5):[23] **4** (200 mg, 0.152 mmol) was dissolved in DCM/TFA (10 mL, 1:1) and stirred for 3 h. Bulk solvent was removed under reduced pressure and the product precipitated from a minimum of methanol over diethyl ether to yield a deep purple crystalline powder (182 mg, 0.127 mmol, 81%). R_F: 0.16 (silica, 8:1:1, acetonitrile/water/$KNO_{3(aq)}$); Rt: 11.0 mins (C-18 silica); ^{1}H NMR (400 MHz, DMSO-d6, 25ºC): δ=9.44 (d, 6H; m-Py-H), 8.99 (d, 6H; o-Py-H, overlapping 8H; β-H), 8.31 (dd, 4H; o-Ar-H, m-Ar-H), 7.87 (d, 3H; NH_3), 4.69 (s, 9H; Py-CH_3), 3.63 (m, 10H; CH_2-CH_2), 3.00 (t, 2H; CH_2-CH_2), -3.06 (s, 2H, NH); ^{13}C{^{1}H} NMR (100 MHz, DMSO-d6, 25ºC): δ=166.68 (C=O), 158.44, 158.14, 157.05, 144.74, 143.61, 134.74, 132.66, 126.61, 126.43, 122.38, 119.40, 116.42, 115.92, 115.28, 70.30, 70.04, 69.55, 67.29, 48.40, 39.18; HRMS (ESI+) m/z [M-3I]$^-$ calcd for $C_{51}H_{50}N_9O_3$: 278.8007 found: 278.8001; UV-Vis (MeOH): λ_{max} 426 (192171), 518 (14154), 555 (6800), 595 (5137), 650 nm (2328 $mol^{-1}dm^3cm^{-1}$).

5-[4-(2-(2-(2-Aminoethoxy)ethoxy)ethaneaminocarbonyl)phenyl]-10,15,20-tris-(4-pyridyl)porphyrin (6): To a solution of **3** (200 mg, 0.220 mmol) in DCM (10 mL) was added TFA (5 mL). The mixture was stirred for 3 h at room temperature. Bulk solvent was removed under reduced pressure and the crude dissolved in a minimum of methanol and precipitated over diethyl ether to give a deep purple solid which was used without further purification (187 mg, 0.207 mmol, 94% yield). R_F: 0.37 (silica, 8:2, DCM/MeOH); ^{1}H NMR (400 MHz, DMSO-d6, 25ºC): δ=9.01 (d, J=4.9 Hz, 6H; o-Py-H), 8.86 (d, J=6.2 Hz, 8H; β-H), 8.28 (m, 4H; o-,m-Ar-H), 8.34 (d, 6H, o-Py-H), 7.92 (s, 1H; N-H), 3.59 (m, 10H; CH_2-CH_2), 3.41 (t, J=5.9 Hz, 2H; CH_2-CH_2), 1.73 (s, 3H; CONH-CH_3), -3.08 (s, 2H; N-H); ^{13}C{^{1}H} NMR (100 MHz, DMSO-d6, 25ºC): δ=169.01(C=O), 149.34, 148.88, 143.11, 134.68, 134.59, 129.69, 126.44, 118.18, 117.93, 70.24,

70.13, 69.52, 57.08, 30.94, 29.73; HRMS (ASAP) m/z $[M+H]^+$ calcd for $C_{48}H_{42}N_9O_3$: 792.3411 found: 792.3403. UV-Vis (MeOH): λ_{max} 405 (112570), 504 (9147), 536 (3166), 582 (2858), 647 nm (1071 $mol^{-1}dm^3cm^{-1}$)

5-[4-(2-(2-(2-Acetimideethoxy)ethoxy)ethaneaminocarbonyl)phenyl]-10,15,20-tris-(4-pyridyl)porphyrin (7): To a solution of **6** (100 mg, 0.111 mmol) in DMF (10 mL) was added DIPEA (5 mL, 3.71 g, 28.7 mmol). Acetic anhydride (2 mL, 2.16 g, 21.16 mmol) was added dropwise and the reaction stirred overnight at room temperature. A second aliquot of acetic anhydride (2 mL, 2.16 g, 21.16 mmol) and DIPEA (5 mL, 3.71 g, 28.7 mmol) was added and the mixture heated to 70 ºC for 4 h with stirring. Bulk solvent was removed under reduced pressure. The crude was taken in DCM and washed with copious amounts of water. The organic layer was separated and dried with anhydrous $MgSO_4$. The semi-crude was dissolved in a minimum of DCM and eluted onto a silica chromatography column. The product eluted in DCM/MeOH (93:7) as the first major red band. The fractions were collected and bulk solvent removed under reduced pressure. The solids were dissolved in a minimum of DCM and precipitated over hexane to yield a deep purple crystalline powder (67 mg, 0.080 mmol, 72% yield). R_F: 0.87 (silica, 95:5, DCM/MeOH); ^1H NMR (400 MHz, DMSO-d6, 25ºC): δ=9.01 (d, J=4.9 Hz, 6H; o-Py-H), 8.86 (d, J=6.2 Hz, 8H; β-H), 8.28 (m, 4H; o-,m-Ar-H), 8.34 (d, 6H, o-Py-H), 7.92 (s, 1H; N-H), 3.59 (m, 10H; CH_2-CH_2), 3.41 (t, J=5.9 Hz, 2H; CH_2-CH_2), 1.73 (s, 3H; NHCO-CH_3), -3.08 (s, 2H; N-H); $^{13}C\{^1H\}$ NMR (100 MHz, DMSO-d6, 25ºC): δ=169.79 (C=O), 149.35, 148.91, 134.71, 129.69, 126.45, 117.96, 70.18, 69.75, 69.52, 23.11 (NHCO-CH_3); HRMS (ESI+) m/z $[M+Na]^+$ calcd for $C_{50}H_{43}N_9O_4{}^{23}Na$: 856.3336 found: 856.3334; UV-Vis (DCM): λ_{max} 425 (126890), 518 (9172), 561 (3322), 595 (3310), 650 nm (1482 $mol^{-1}dm^3cm^{-1}$).

5-[4-(2-(2-(2-Acetimideethoxy)ethoxy)ethaneaminocarbonyl)phenyl]-10,15,20-tris-(N-methyl-4-pyridinium)porphyrin trichloride (8): 7 (50 mg, 0.060 mmol) was dissolved in DMF (80 mL) and the flask fitted with a triethylamine trap bubbler. Methyl iodide (1 mL) was added dropwise and the reaction stirred at 40 ºC overnight. Excess diethyl ether (100 mL) as added to the flask and the precipitate filtered off under gravity through a plug of cotton wool. The crude precipitate was dissolved in methanol and precipitated from diethyl ether (100 mL). The product was filtered under reduced pressure to give a burgundy solid which was washed copiously with diethyl ether to yield the product as a deep purple crystalline solid as the triiodide salt. The product was dissolved in water (5 mL) and excess ammonium hexafluorophosphate added, the precipitate was collected via filtraction under reduced pressure, the solids were dissolved in acetone (5 mL) and excess tetrabutylammonium chloride added, the precipitate was collected via filtration under reduced pressdure and the solids dried until reaching constant mass to yield a deep purple powder (56 mg, 0.056 mmol, 94% yield). R_F: 0.34 (silica, 8:1:1, acetonitrile/water/$KNO_{3(aq)}$); Rt: 10.10 mins (C-18 silica); ^{1}H NMR (400 MHz, DMSO-d6, 25ºC): δ=9.45 (d, J=6.5 Hz, 6H; m-Py-H), 9.15 (s, 4H; o-Py-H), 9.04 (s, 2H; o-Py-H), 8.98 (d, J=6.5 Hz, 8H; β-H), 8.31 (d, J=5.7 Hz, 4H; o-,m-Ar-H), 7.93 (s, 1H; N-H), 4.68 (s, 9H; Py-CH_3), 3.60 (m, 8H; CH_2-CH_2), 3.42 (t, 2H; CH_2-CH_2), 3.18 (m, 2H, CH_2-CH_2), 1.77 (s, 3H; NHCO-CH_3), -3.08 (s, 2H; N-H); ^{13}C{^{1}H} NMR (100 MHz, DMSO-d6, 25ºC): δ= δ=169.84 (C=O), 166.63 (C=O), 157.16, 144.73, 142.96, 134.74, 132.65, 126.61, 122.40, 115.93, 114.9, 70.15, 69.73, 69.56, 48.42 (Py-$\underline{C}H_3$), 34.91, 23.14 (NHCO-CH_3); HRMS (ESI+) m/z $[M-3Cl]^{3+}$ calcd for $C_{53}H_{52}N_9O_4$: 292.8042 found: 292.8047; UV-Vis (H_2O): λ_{max} 423 (125893), 521 (8913), 562 (4677), 588 (4365), 645 nm (1479 $mol^{-1}dm^3cm^{-1}$); Fluorescence: (H_2O): λ_{ex} 425 nm, λ_{em} 658, 714 nm.

Conjugate (9): 5 (49 mg, 0.096 mmol) and TBTU (31 mg, 0.097 mmol) were suspended in DMSO (1 ml) followed by the addition of DIPEA (49 µL, 0.286 mmol). The mixture was stirred for 5 min followed by the addition of **1** (40 mg, 0.032 mmol) (a 3:1 ratio of **5** and **1** was utilised to push amide formation with **1** to completion as a 1:1 ratio was found to result in quantities of unreacted **1**). The dark coloured mixture was stirred for 3 h whilst protected from light then diluted with acetone (12 mL) and left to stand for 13 h at 4°C, the precipitate was collected by centrifugation. The collected solid residue was suspended in acetone (10 mL) and the solids collected by centrifugation. The combined solids were dried under reduced pressure then dissolved in H_2O (0.5 mL) followed by the addition of a solution of NH_4PF_6 (31 mg, 0.190 mmol) in H_2O (0.5 mL) to yield a precipitate that was collected by centrifugation. The solids were taken in H_2O (3 mL) then collected by centrifugation. The collected solid was dried under reduced pressure then dissolved in acetone (2.5 mL) followed by the addition of a solution of tetrabutylammonium chloride (93 mg, 0.335 mmol) in acetone (0.5 mL). The precipitate was collected by centrifugation then the collected solid dispersed in acetone (1 mL) and collected by centrifugation. The solid was suspended in acetone:H_2O (9:1, 10 mL) and the insoluble material collected by centrifugation. The collected solid was then dissolved in H_2O (1 mL) followed by the addition of acetone (9 mL), the mixture was vigorously shaken then allowed to stand for 30 min, followed by centrifugation to collect the solid. This process was repeated followed by washing of the collected solid in acetone (3 x 10 mL) and collection by centrifugation. The solid was dissolved in H_2O (1 mL) then lyophilized to yield a purple solid (8 mg, 5.51 µmol, 17% yield). R_F: 0.32 (silica, 8:1:1, acetonitrile/water/$KNO_{3(aq)}$); ^{1}H-NMR (400 MHz, DMSO-d6, 25ºC): δ=9.44 (m, 6H; m-Py-H), 9.07 (m, 6H; o-Py-H), 8.96 (m, 8H; β-H, overlapping 2H, N<u>H</u>-CO, 8.30 (m, 4H; o-,m-Ar), 5.76-

5.87 (m, 4H; Ru-Ar), 4.68 (s, 9H; Py-CH_3), 4.32 (s, 6H; PTA), 3.95 (s, 6H; PTA), 3.56 (m, 12H; CH_2-CH_2), 1.84 (s, 3H; Ar-CH_3) (-CH_2CH_2-Ar- signal not observed as this is obscured by residual solvent signal); ^{31}P-NMR (162 MHz, D_2O, 25ºC): δ=-33.76 (s, PTA). $^{13}C\{^1H\}$ NMR (100 MHz, DMSO-d6, 25ºC): δ=173.02 (C=O), 169.80 (C=O), 164.44, 157.15, 143.86, 132.86, 125.38, 121.63, 114.85, 114.60, 86.72, 85.11, 70.06, 69.42, 68.55, 48.38, 47.93, 47.79, 39.66, 38.90, 34.36, 26.75; HRMS (ESI+) m/z $[M]^{3+}$ calcd for $C_{69}H_{72}N_{12}O_8PRu$: 443.1458 found: 443.1446; UV-Vis (H_2O): λ_{max} 426 (131825), 525 (7943), 565 (4571), 595 (3388), 650 nm (1047 $mol^{-1}dm^3cm^{-1}$). ; Fluorescence: (H_2O): λ_{ex} 426 nm, λ_{em} 656, 710 nm.

RESULTS AND DISCUSSION

Synthesis of an Amine Reactive RAPTA Complex

The synthesis of the [Ru(η^6-arene)(C_2O_4)PTA] complexes was achieved using previously reported methodology.[24] The known complex **1**, bearing a pendant carboxylic acid functionality, was chosen as it provides a route by which it can be conjugated to a porphyrin bearing a pendant amine group. Additionally, the use of the oxalate ligand within these complexes confers good aqueous solubility[25] whilst acting as a protecting group in amide-forming reactions. (Scheme 1: **1**, **2**).

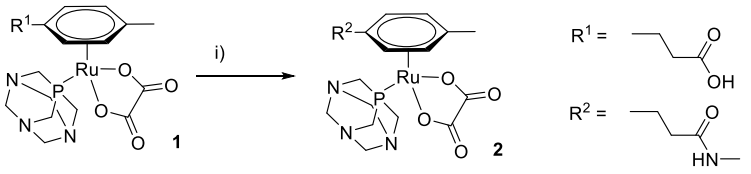

Scheme 1. Synthesis of a second-generation oxalate RAPTA complex. Conditions used: i) TBTU, DIPEA, DMSO then CH_3NH_2.HCl, RT, 2h.

Synthesis of a Carboxylic Acid Reactive Porphyrin

The synthesis of **5** was carried out by adopting the method described by Yap *et al*.[23] Briefly, the synthesis of the initial free base porphyrin was carried out by a mixed aldehyde [3+1] condensation under Adler-Longo conditions in refluxing propionic acid with pyrrole giving the porphyrin as a lustrous purple crystalline solid in good yield (4.5%) after column chromatography. This reaction could be scaled by a factor of 2 increasing the mass yield of the reaction to near gram scale (Scheme 2). The methyl ester was readily saponified in basic THF/MeOH media with heating for 48 h giving the carboxylic acid porphyrin in near quantitative yield (98%) after aqueous work-up. Conjugation to a Boc-protected hydrophilic bifunctional PEG linker took place in DMF with 2-(1H-benzotriazole-1-yl)-1,1,3,3-tetramethylaminium tetrafluoroborate (TBTU) and *N*,*N*-diisopropylethylamine (DIPEA) with heating overnight. The porphyrin **3** was afforded in an excellent yield (84%) after column chromatography. Notably, the addition of this PEG spacer produced a porphyrin which was soluble in methanol and ethanol. Quarternisation of the pyridyl moieties gave the cationic water-soluble N-methyl-4-pyridinium groups (**4**) with iodide as the counter ion after reaction with methyl iodide in DMF with heating overnight. Finally, **4** was deprotected with DCM/TFA (1:1) to give **5** in 81%. Synthesis of **3** was repeated, which was found to be highly reproducible. **3** was de-protected with DCM/TFA (1:1). The amine salt (**6**) was reacted with acetic anhydride under anhydrous basic conditions and purified by column chromatography to give the product **7** in 72% yield. Following this, the porphyrin was rendered water-soluble, again, by methylation of the pyridyl groups in DMF with the aid of methyl iodide. The product

was converted from the iodide salt to the hexafluorophosphate salt by dissolving in methanol with the addition of ammonium hexafluorophosphate to give the novel product **8**.

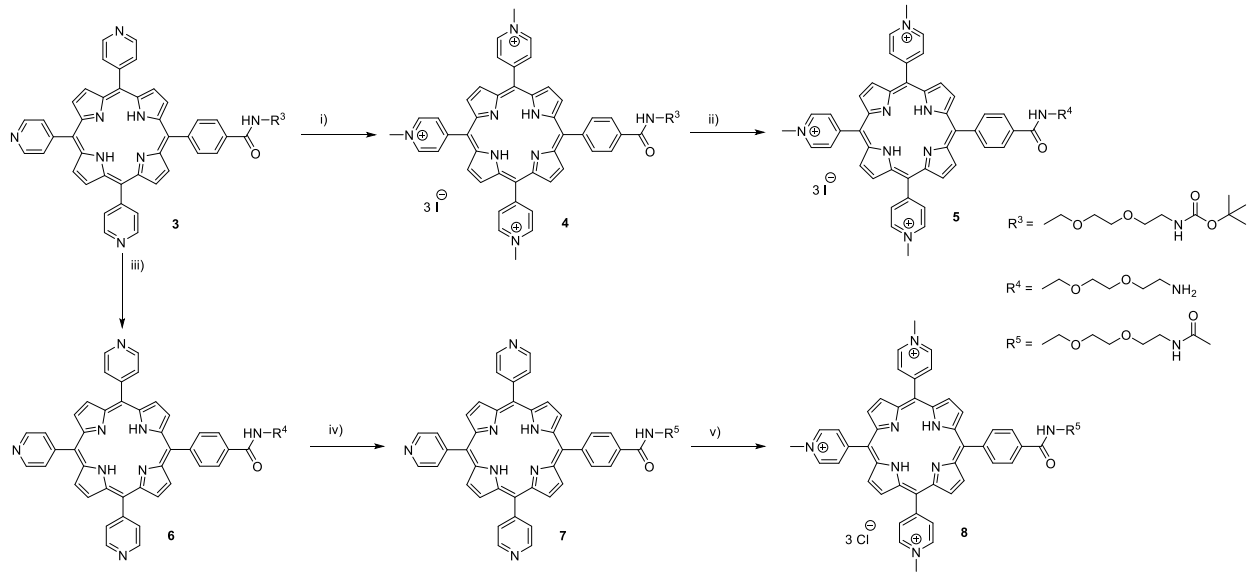

Scheme 2. Synthesis of a water-soluble porphyrin with a hydrophilic PEG spacer and alkyl amine conjugatable handle. Conditions used: i) MeI, DMF, Ar, 40 ºC, stir 17 h. ii) TFA/DCM (1:1), RT, stir 1 hr. iii) TFA/DCM (1:1), RT, stir 1 h. iv) Ac_2O, DIPEA, DMF, Ar, 40 ºC, stir 17 h. v) MeI, DMF, Ar, 40 ºC, stir 17 h.

RAPTA-Porphyrin Conjugation

The synthesis of the conjugate was carried out via peptide coupling utilizing DMSO as solvent, and TBTU and DIPEA as coupling reagents (Scheme 3: **9**). The conjugate was purified firstly by liquid-liquid extraction and isolated by centrifugation, followed by counter-ion exchange to yield the more water-soluble trichloride salt of **9**. The novel RAPTA-porphyrin conjugate (**9**) was found to be highly soluble in DMSO, water, and biological media. Interestingly, the NMR spectrum of **9**

recorded in DMSO-d_6 revealed signals corresponding to the η^6-arene protons in the expected region at ~5.8 ppm. However, in D_2O these signals are shifted downfield to ~7.3. The origins of these differences are likely to be related to different conformations of the conjugate in these solvents.

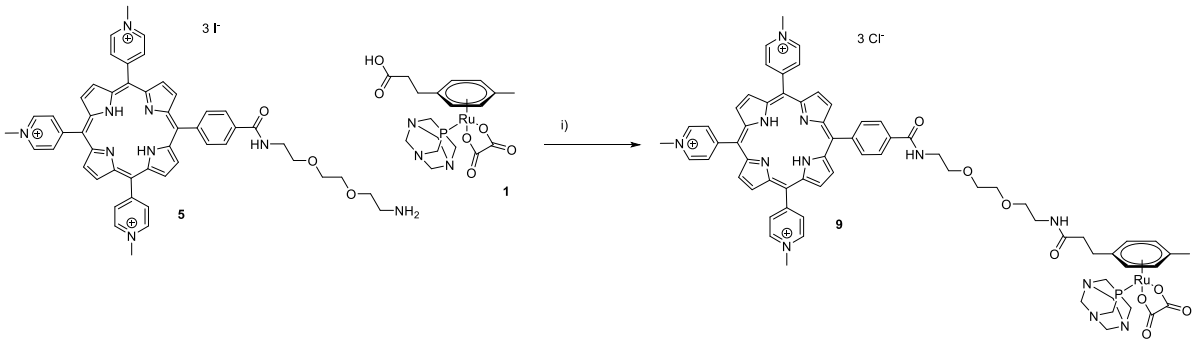

Scheme 3. Synthesis of a water-soluble second-generation cationic RAPTA-porphyrin conjugate. Conditions used: i) TBTU, DIPEA, DMSO, Ar, stir 3 h.

UV-Vis and Fluorescence

Ideally, a photodynamic sensitizer should absorb in the red-NIR region for deep tissue penetration, however, the use of optical fibers which can be inserted into the body can negate this requirement somewhat. Conjugation of **2** to the porphyrin did not deleteriously alter the porphyrins optoelectronic properties. The results of the UV-Vis absorption studies for the porphyrins **8** and the conjugate **9** are shown in Figure S1 (supplementary information) and Table 1 recorded at room temperature in water. The conjugate was maintained as the free-base rather than undergoing complexation with a heavy-metal such as Pt^{2+} or Pd^{2+} in order to preserve the Q-bands in order to profit from the favorable red/NIR absorption band at 650 nm

The Soret bands (*ca.* 420 nm) were found to have the highest molar absorptivity coefficient, while the Q-bands had the lowest. The highest wavelength absorptions were at *ca.* 650 nm. As expected, the tabulated results are extremely similar for **8** and **9**, suggesting no, or minimal, electronic interaction between the porphyrin and RAPTA components.

Table 1. UV-Vis absorption maxima (nm) and molar absorptivity coefficients determined in H_2O. Molar absorptivity coefficients are given as $\log_{10}$ values in brackets.

Entry	Soret band	Q band I	Q band II	Q band III	Q band IV
8	425 (5.10)	518 (3.95)	561 (3.67)	595 (3.64)	649 (3.17)
9	426 (5.12)	525 (3.90)	565 (3.66)	595 (3.53)	650 (3.02)

Fluorescence spectra were recorded and, once again, the presence of the RAPTA group did not deleteriously affect the normalized fluorescence spectra, suggesting no significant excited state perturbations occur upon conjugation (Figure S2; supplementary information).

The excitation and emission wavelengths ($\lambda_{ex}/\lambda_{em}$) were found to be 425/658 and 426/656 respectively for **8** and **9** (Table 2).

Table 2. Excitation, emission, and Stokes shift measurements for compounds **8** and **9** obtained in H_2O.

Entry	Solvent	λ_{ex} (nm)	λ_{em} (nm)	Stokes shift (nm)
8	Water	425	658	233
9	Water	426	656	231

Relative Singlet Oxygen Quantum Yield

The relative singlet oxygen quantum yield is a measure of the efficiency of a photosensitizer to convert triplet state molecular oxygen into highly cytotoxic singlet oxygen. 9,10-anthracenediyl-bis(methylene)dimalonic acid, (ABDA), is commonly used as a diagnostic tool in which photo-oxidation of the central arene ring takes place when in the presence of singlet oxygen yielding an endoperoxide and a reduction in UV-Vis absorption spectra relative to a control. We followed the method according to Senge *et al*.[26] In this case, the water soluble photosensitizer *meso*-tetra(N-methyl-4-pyridyl)porphyrin (**TMePyP**) was used as a standard during singlet oxygen quantum yield experiments. The results of the irradiation of ABDA (absorption monitored at 380 nm) with time are shown in Figure S3 (supplementary information). Qualitatively, a decrease in the absorption maxima corresponds to the production of singlet oxygen. It can clearly be seen that a decrease in the absorbance signal of ABDA can be seen over time when irradiated with red light (617-651 nm, 1035.8 Wm^{-2}). This is an indication that singlet oxygen is being produced. Irradiation of ABDA in the absence of a photosensitizer did not produce any statistically significant indication singlet oxygen. The relative singlet oxygen quantum yields of **8** and **9** were then calculated relative to that of **TMePyP**. **8** gave a value of 0.96 (relative to a normalized value of 1 for **TMePyP**), however **9** gave a value of 1.57, this value could be attributed to steric hindrance of the ruthenium component minimizing porphyrin aggregation (Table 3). It is well understood that even water-soluble cationic porphyrins aggregate and π-π stack in solution which limits their relative singlet oxygen quantum yields, possibly explaining the differential between **8** and **9**.

Table 3. Data for the relative singlet oxygen quantum yields (Φ_Δ) for given compounds obtained by photochemical studies by time-course UV-Vis spectroscopy with the presence of a singlet oxygen radical trap (ABDA). n=3.

Entry	Φ_Δ
ABDA	-
TMePyP	1.00
8	0.96
9	1.57

Photostability

Photostability is a major concern for any photosensitizer/fluorophore, as small molecule fluorophores often experience irreversible photobleaching upon continuous illumination with light, therefore, limiting their use in biomedical applications. The photostability of **8** and **9** was investigated with Rose Bengal being utilized as a non-porphyrin control for samples irradiated with white light, and **TMePyP** being used as a control for samples irradiated with red light. When irradiated continuously for 60 minutes in H_2O, **8**, **9**, and **TMePyP** were all found to behave similarly (Figure 1). Previous studies have also demonstrated that the tetrapyrrolic core has been found to be appreciably photostable.[27] None of the samples were found to have a normalized absorbance of less than 95% after irradiation with red light for 60 minutes. When irradiated continuously with white light for 10 minutes in H_2O, **8** and **9** were both found to be appreciably photostable with normalized absorbance values of 88.65±0.03% (n=3) and 86.60±0.01% (n=3) respectively, which did not deviate significantly from the normalized absorbance when irradiated continuously for 60 minutes with red light. Meanwhile, the commercially available Rose Bengal control was found to fully photobleach to a normalized absorbance value of 1.58±0.01% (n=3) after continuous irradiation with white light for 10 minutes. Therefore, compared to the commercially available photosensitizer/fluorophore, the porphyrin-RAPTA conjugate can be said to be relatively photostable under these specific conditions.

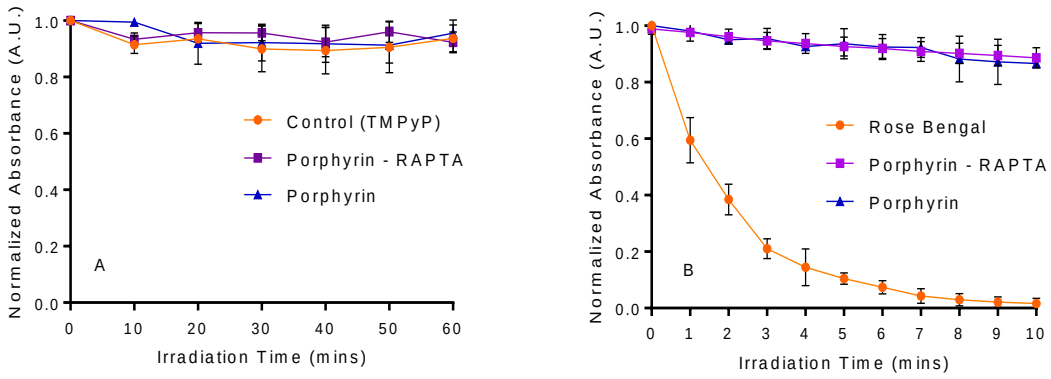

Figure 1. (A) Photostability studies of compounds **8**, **9** and **TMePyP** irradiated continuously with red light (617-651 nm, 1035.8 W m^{-2}) monitored at 650 nm. (B) Photostability studies of compounds **8**, **9** (monitored at 650 nm) and **Rose Bengal** (monitored at 560 nm) irradiated continuously with white light (400-1200 nm). Data are presented as X±SD (n=3).

In order to probe the photostability of the [Ru(η^6-arene)(C_2O_4)PTA] complex we took a known mass of **9** into D_2O (0.7 mL) in an NMR tube and recorded the $^{31}P\{^1H\}$ NMR and ^1H NMR spectra at room temperature. The sample was protected from light, then irradiated sequentially in 20 J cm^{-2} increments of white light (400-1200 nm) and the NMR spectrum was recorded after each irradiation. With regards to the $^{31}P\{^1H\}$ NMR spectra, the relative intensity of the peak originating from the bound PTA ligand did not increase or decrease after irradiation with white light, furthermore, no other peaks were observed even at high doses of 60 J cm^{-2} as seen in Figure S4 (supplementary information). Again, the ^1H NMR remained unchanged. These data suggests that no significant changes to the Ru(II) ligands were occurring in solution after irradiation with white light. Therefore, we are confident that this unique conjugate consists of not only a photostable tetrapyrrole, but, also a stable RAPTA moiety. It is interesting to note that these results contrast with those reported in related systems[28,29] where ligand loss, and therefore activation of the

metallodrug, in half-sandwich Ru(II)-η^6-arene complexes was observed on irradiation of aqueous solutions of the complexes. Clearly under the experimental conditions utilized here **9** is stable and the enhanced stability compared to literature reports may be related to differences in irradiation times and the radiation wavelengths employed in these experiments.

In Vitro Anticancer Activity

In order to determine the biological anticancer efficacy of **2**, **8**, and **9**, we chose to examine these compounds in the human Caucasian colorectal adenocarcinoma (HT-29) cell line, chosen as a model of colorectal cancers which are the third most common cancers worldwide, where 20% of cases suffer from metastases and 56% of patients with colorectal cancers die from this disease.[30] Cells were treated with varying concentrations and a fixed dose of light (20 J cm^{-1}) over two incubation time periods (24 h and 48 h) and cell-viability was determined by an MTT assay (Figure 2). The 96-well plates were washed and replenished with fresh media, to remove any unbound or non-internalized compound, before irradiation with a fixed dose of white light. The RAPTA-porphyrin conjugate **9** had an incubation time-dependent cell viability response. At the 24 h incubation time period, **8** was found to have no impact on cell viability, but acted as a viable photosensitizer in its own right when irradiated with white light (20 J cm^{-2}). With regards to **2**, an IC_{50} was not observed even at a concentration of 500 μM. As expected, no statistically significant light-dependent effect on cell viability was observed with this RAPTA species. Interestingly, we observed a significant decrease in cell viability in the 'dark' for conjugate **9** compared to complex **2**. Covalent tethering of the porphyrin to the RAPTA complex resulted in a 10-fold decrease in the concentration of Ru(II) required to achieve a cell viability of ~70%. We attribute this decrease in

cell viability to the natural ability of the cationic porphyrin to internalize the RAPTA compared to **2** alone (cellular uptake experiments are described later). Comparing this with the 48 h incubation, we observed a decrease in the viability of cells treated with **2**, and again with no light dependence on activity observed. **8** has increasing impact on cell viability at higher concentrations in the 'dark', while still producing a statistically significant difference compared to the irradiated cells. Most interestingly, **9** gave a cell viability of 16.8±2.0% (n=3) when the cells were incubated for 48 h with 10 μM compared to a cell viability of 14.9±1.7% (n=3) when incubated for 24 h with 250 μM, representing a 25-fold decrease in effective concentration for a statistically comparable result at the expense of a longer incubation period (Figure 2). With irradiation of light, we observed a cell viability 2.3 ±1.2% (n=3) using a 10 μM concentration and an incubation period of 48 h for conjugate **9**. Alternatively, when not irradiated, after incubation for 48 h, **9** gave a cell-viability of 16.8 ± 2.0% (n=3), while **2** gave a cell viability of 42.8 ± 3.9% (n=3) at the 10 μM concentration level, representing a significant improvement in the anticancer activity by conjugation of the RAPTA metallodrug to the porphyrin motif. For **2** and **9** it is expected that under the incubation conditions of this experiment that the ruthenium centre will be activated through oxalato ligand exchange, as reported for an isostructural ruthenium centre in a previous study.[24] The loss of the bidentate oxalato ligand, that acts as a protecting group to prevent ruthenium-centred reactivity, 'activates' the complex to a form able to metallate intracellular biomacromolecules that results in the observed anticancer activity.[24] It is important to note that these data have been obtained after a maximum incubation period of 48 h, while similar values were obtained with four times the amount of ruthenium atoms whilst requiring a 72 h incubation period.[16, 17]

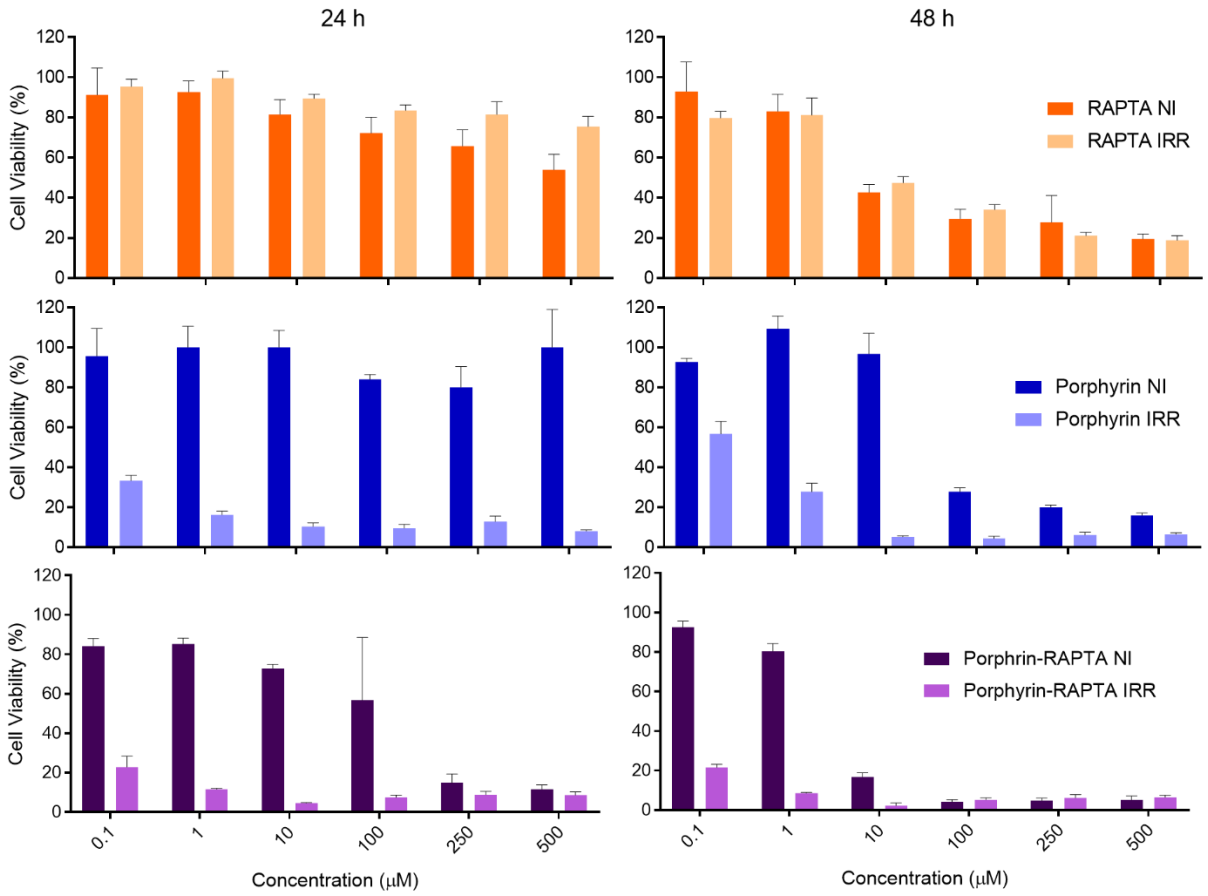

Figure 2. Temporal MTT assay of **2** (top), **8** (middle) and **9** (bottom) displaying time-dependent and concentration-dependent cell viabilities with 0 J cm^{-1} and 20 J cm^{-1} light doses. Data are presented as X±SD (n=3). 2-way ANOVA statistical analysis was carried out with Bonferroni's *post-hoc* multiple comparisons significance testing. NI; not irradiated; IRR; irradiated (20 J cm^{-2}).

Fluorescence Imaging

As well as being known for their photosensitizing properties, porphyrins are in their own right excellent fluorophores which allows monitoring of their *in vitro* and *in vivo* biodistribution and cell-uptake by fluorescence imaging. The conjugate, **9**, is intrinsically fluorescent, meaning that

further synthetic functionalization was not required. Cellular uptake studies were carried out with (**9**) and control compound (**8**) according to the methods of Boyle *et al* to determine whether or not internalization was occuring.[14] Both 10 μM of **8** and **9** were incubated with HT-29 for 24 h. Diffuse fluorescence could clearly be observed emanating from within the sub-cellular environment by fluorescence microscopy, as seen in Figure S5 (supplementary information). While the compounds clearly were being internalized, only diffuse fluorescence from **8** and **9** could be observed suggesting that at the dose of 10 μM the conjugate is not specifically localized within any given cellular organelle. In the case of both **8** and **9**, brightfield micrographs also provide qualitative morphological evidence of porphyrin photosensitization indicated by blebbing of cells which is indicative of early onset apoptosis due to activation of the photosensitizer from the microscope light source.

ICP-MS

Inductively coupled plasma mass spectrometry was used as a highly sensitive technique to quantify the relative concentrations of ^{101}Ru in HT-29 cells that had been incubated with compounds **2** or **9** for 48 h, followed by washing, harvesting, and re-suspending the cells in PBS. The protocol was developed support whether **2** or **9** had been internalized by HT-29 cells (Figure 3). We predicted that due to the natural ability of N-methylpyridinium functionalized porphyrin to be internalized by cancer cells that the relative concentrations of ^{101}Ru in the HT-29 cells should be higher due to the ability of the porphyrin to chaperone the RAPTA metallodrug into the cell through the predominately negatively charged cell membrane. The results unequivocally indicated that the concentration of ^{101}Ru was significantly higher ($p<0.01$) for cells that were treated with

10 μM of **9** compared to 10 μM of **2** and compared to the cell only sample (vehicle controlled). Combined with the fluorescence data described above the porphyrin-RAPTA conjugate is significantly more internalized by the HT-29 cells, relative to unconjugated **2**, even at an active dose.

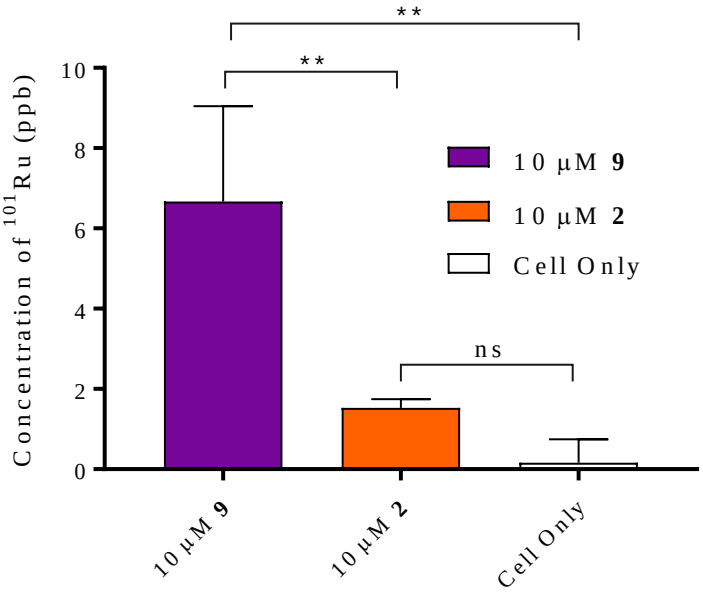

Figure 3. ICP-MS data highlighting the concentration of ^{101}Ru (ppb) in HT-29 cells incubated with 10 μM for 48 h. Data are presented as X±SD (n=3). An ordinary ANOVA statistical analysis was carried out with Dunnett's *post-hoc* multiple comparisons significance testing, ns; ($p>0.05$), *; ($p<0.05$), **; ($p<0.01$).

Conclusion

To conclude, we have successfully synthesized a second-generation water-soluble porphyrin-RAPTA conjugate and evaluated its photochemical and biological properties. The photostability of the porphyrin component of the conjugate was found to be good, regardless of whether it was irradiated with white light or red light, and the conjugate retained its ground and excited state

properties relative to the non-conjugated porphyrin. Furthermore, it exhibited a relatively higher singlet oxygen quantum yield compared to a known porphyrin standard. Biological evaluation has allowed us to determine that the conjugate is a viable photosensitizer in its own right, but it also operates as an anticancer agent by controlling cell proliferation in the 'dark' at low concentrations (10 μM), while **2** alone had an IC_{50} >500 μM. In fact, a 2.5-fold decrease in cell viability was observed when compared to **2** alone at the same concentration in the 'dark'. Furthermore, we obtained this data at shorter incubation times (48 h), while previous work on porphyrin-ruthenium conjugates, and RAPTA compounds, have required 72 h incubations in order to achieve acceptable IC values. Fluorescence microscopy and ICP-MS has allowed us to study cellular uptake, from which we attribute the enhanced anticancer efficacy of this conjugate to the natural ability of the cationic porphyrin to increase the effective concentration of the ruthenium metallodrug internalized in the cell through its internalization characteristics. We can therefore envisage such porphyrin-RAPTA conjugates having clinical potential for the combined therapy of solid tumours; with localized light treatment being used to generate cytotoxic reactive oxygen species via the porphyrin, and the RAPTA component inhibiting growth of any tumor cells which escape photodynamic destruction. We believe, that these studies have demonstrated that porphyrin-RAPTA conjugates have to potential to be clinically viable, and that we have laid the foundation for further studies to closer examine the biological efficacy of these conjugates *in vivo*.

AUTHOR INFORMATION

Corresponding Authors

Prof. R. W. Boyle.* e-mail: r.w.boyle@hull.ac.uk

Dr B. S. Murray.* e-mail: b.s.murray@hull.ac.uk

Author Contributions

The manuscript was written through contributions of all authors. All authors have given approval to the final version of the manuscript.

Acknowledgements

The authors thank the EPSRC UK National Mass Spectrometry Facility at Swansea University for the acquisition of mass spectrometry data.

Appendix A. SUPPLEMENTARY DATA

The supplementary data section contains the characterization data (NMR, MS, UV-Vis spectra, and HPLC traces) for all synthesized ruthenium and porphyrin compounds where possible, and brightfield and fluorescence micrographs.

Notes

The authors declare no competing financial interests.

REFERENCES

1 Scolaro, C.; Bergamo, A.; Brescacin, L.; Delfino, R.; Cocchietto, M.; Laurenczy, G.; Geldbach, T. J.; Sava, G.; Dyson, P. J. In Vitro and in Vivo Evaluation of Ruthenium(II)-Arene PTA Complexes. *J. Med. Chem.* **2005**, *48*, 4161–4171.

2 Murray, B. S.; Babak, M. V; Hartinger, C. G.; Dyson, P. J. The Development of RAPTA Compounds for the Treatment of Tumors. *Coord. Chem. Rev.* **2016**, *306*, 86–114.

3 Meier, S. M.; Kreutz, D.; Winter, L.; Klose, M. H. M.; Cseh, K.; Weiss, T.; Bileck, A.; Alte, B.; Mader, J. C.; Jana, S.; Chatterjee, A.; Bhattacharyya, A.; Hejl, M.; Jakupec, M. A.; Heffeter, P.; Berger, W.; Hartinger, C. G.; Keppler, B. K.; Wiche, G.; Gerner, C. An Organoruthenium Anticancer Agent Shows Unexpected Target Selectivity For Plectin. *Angew. Chemie - Int. Ed.* **2017**, *56*, 8267–8271.

4 Wolters, D. A.; Stefanopoulou, M.; Dyson, P. J.; Groessl, M. Combination of Metallomics and Proteomics to Study the Effects of the Metallodrug RAPTA-T on Human Cancer Cells. *Metallomics* **2012**, *4*, 1185–1196.

5 Oun, R.; E. Moussa, Y.; Wheate, N. J. The Side Effects of Platinum-Based Chemotherapy Drugs: A Review for Chemists. *Dalt. Trans.* **2018**, *47*, 6635–6870.

6 Shen, D. W.; Pouliot, L. M.; Hall, M. D.; Gottesman, M. M. Cisplatin Resistance: A Cellular Self-Defense Mechanism Resulting from Multiple Epigenetic and Genetic Changes. *Pharmacol. Rev.* **2012**, *64*, 706–721.

7 Wang, F.; Habtemariam, A.; Van Der Geer, E. P. L.; Fernández, R.; Melchart, M.; Deeth, R. J.; Aird, R.; Guichard, S.; Fabbiani, F. P. A.; Lozano-Casal, P.; Oswald, I. D. H.; Jodrell, D. I.; Parsons, S.; Sadler, P. J. Controlling Ligand Substitution Reactions of Organometallic Complexes: Tuning Cancer Cell Cytotoxicity. *Proc. Natl. Acad. Sci. U. S. A.* **2005**, *102*, 18269–18274.

8 Weiss, A.; Berndsen, R. H.; Dubois, M.; Muller, C.; Schibli, R.; Griffioen, A. W.; Dyson,

P. J.; Nowak-Sillwinska, P. In vivo anti-tumor activity of the organometallic ruthenium(ii)-arene complex [Ru(η ^{6}-p-cymene)Cl_2(pta)] (RAPTA-C) in human ovarian and colorectal carcinomas *Chem. Sci.* **2014**, *5*, 4742–4748.

9 Josefsen, L. B.; Boyle, R. W. Unique Diagnostic and Therapeutic Roles of Porphyrins and Phthalocyanines in Photodynamic Therapy, Imaging and Theranostics. *Theranostics* **2012**, *2*, 916–966.

10 Sandland, J.; Malatesti, N.; Boyle, R. Porphyrins and Related Macrocycles: Combining Photosensitization with Radio- or Optical-Imaging for next Generation Theranostic Agents. *Photodiagnosis Photodyn. Ther.* **2018**, *23*, 281–294.

11 Allison, R. R.; Sibata, C. H. Oncologic Photodynamic Therapy Photosensitizers: A Clinical Review. *Photodiagnosis Photodyn. Ther.* **2010**, *7*, 61–75.

12 Danhier, F. To Exploit the Tumor Microenvironment: Since the EPR Effect Fails in the Clinic, What Is the Future of Nanomedicine? *J. Control. Release.* **2016**, *244*, 108–121.

13 Maeda, H. Macromolecular Therapeutics in Cancer Treatment: The EPR Effect and Beyond. *J. Control. Release.* **2012**, *164*, 138–144.

14 Entract, G. M.; Bryden, F.; Domarkas, J.; Savoie, H.; Allott, L.; Archibald, S. J.; Cawthorne, C.; Boyle, R. W. Development of PDT/PET Theranostics: Synthesis and Biological Evaluation of an 18F-Radiolabeled Water-Soluble Porphyrin. *Mol. Pharm.* **2015**, *12*, 4414–4423.

15 Golombek, S. K.; May, J. N.; Theek, B.; Appold, L.; Drude, N.; Kiessling, F.; Lammers,

T. Tumor Targeting via EPR: Strategies to Enhance Patient Responses. *Adv. Drug Deliv. Rev.* **2018**, *130*, 17–38.

16 Schmitt, F.; Govindaswamy, P.; Zava, O.; Suss-Fink, G.; Juillerat-Jeanneret, L.; Therrien, B. Combined Arene Ruthenium Porphyrins as Chemotherapeutics and Photosensitizers for Cancer Therapy. *J. Biol. Inorg. Chem.* **2009**, *14*, 101–109.

17 Gianferrara, T.; Bergamo, A.; Bratsos, I.; Milani, B.; Spagnul, C.; Sava, G. Ruthenium - Porphyrin Conjugates with Cytotoxic and Phototoxic Antitumor Activity. *J. Med. Chem.* **2010**, *53*, 4678–4690.

18 Rapozzi, V.; Zorzet, S.; Zacchigna, M.; Della Pietra, E.; Cogoi, S.; Xodo, L. E. Anticancer Activity of Cationic Porphyrins in Melanoma Tumour-Bearing Mice and Mechanistic in Vitro Studies. *Mol. Cancer* **2014**, *13*, 1–17.

19 Hammerer, F.; Poyer, F.; Fourmois, L.; Chen, S.; Garcia, G.; Teulade-Fichou, M. P.; Maillard, P.; Mahuteau-Betzer, F. Mitochondria-Targeted Cationic Porphyrin-Triphenylamine Hybrids for Enhanced Two-Photon Photodynamic Therapy. *Bioorganic Med. Chem.* **2018**, *26*, 107–118.

20 Odeh, A. M.; Craik, J. D.; Ezzeddine, R.; Tovmasyan, A.; Batinic-haberle, I.; Benov, L. T. Targeting Mitochondria by Zn(II) N-Alkylpyridylporphyrins: The Impact of Compound Sub- Mitochondrial Partition on Cell Respiration and Overall Photodynamic Efficacy. *PLoS One* **2014**, *9*, 1-9.

21 Ricchelli, F.; Franchi, L.; Miotto, G.; Borsetto, L.; Gobbo, S.; Nikolov, P.; Bommer, J. C.; Reddi, E. Meso-Substituted Tetra-Cationic Porphyrins Photosensitize the Death of Human

Fibrosarcoma Cells via Lysosomal Targeting. *Int. J. Biochem. Cell Biol.* **2005**, *37*, 306–319.

22 Tsubone, T. M.; Martins, W. K.; Pavani, C.; Junqueira, H. C.; Itri, R.; Baptista, M. S. Enhanced Efficiency of Cell Death by Lysosome-Specific Photodamage. *Sci. Rep.* **2017**, *7*, 1–19.

23 Yap, S. Y.; Price, T. W.; Savoie, H.; Boyle, R. W.; Stasiuk, G. J. Selective Radiolabelling with ^{68}Ga under Mild Conditions : A Route towards a Porphyrin PET/PDT Theranostic Agent. *Chem. Commun.* **2018**, *54*, 7952–7954.

24 Murray, B. S.; Menin, L.; Scopelliti, R.; Dyson, P. J. Conformational Control of Anticancer Activity: The Application of Arene-linked Dinuclear Ruthenium(II) Organometallics *Chem. Sci.* **2014**, *5*, 2536–2545.

25 Ang, W. H.; Daldini, E.; Scolaro, C.; Scopelliti, R.; Juillerat-jeannerat, L.; Dyson, P. J. Development of Organometallic Ruthenium−Arene Anticancer Drugs That Resist Hydrolysis. *Inorg. Chem.* **2006**, *45*, 9006–9013.

26 Belali, S.; Savoie, H.; Brien, J. M. O.; Cafolla, A. A.; Connell, B. O.; Karimi, A. R.; Boyle, R. W.; Senge, M. O. Synthesis and Characterization of Temperature- Sensitive and Chemically Cross-Linked Poly(N- Isopropylacrylamide)/Photosensitizer Hydrogels for Applications in Photodynamic Therapy. *Biomacromolecules* **2018**, *19*, 1592–1601.

27 Merchán, M.; Ouk, T. S.; Kubát, P.; Lang, K.; Coelho, C.; Verney, V.; Commereuc, S.; Leroux, F.; Sol, V.; Taviot-Guého, C. Photostability and Photobactericidal Properties of Porphyrin-Layered Double Hydroxide-Polyurethane Composite Films. *J. Mater. Chem. B*

2013, *1*, 2139–2146.

28 Basu, U.; Karges, J.; Chotard, F.; Balan, C.; Le Gendre, P.; Gasser, G.; Bodio, E.; Malacea Kabbara, R. Investigation of Photo-Activation on Ruthenium(II)–Arene Complexes for the Discovery of Potential Selective Cytotoxic Agents. *Polyhedron* **2019**, *172*, 22–27.

29 Renfrew, A. K.; Karges, J.; Scopelliti, R.; Bobbink, F. D.; Nowak-Sliwinska, P.; Gasser, G.; Dyson, P. J. Towards Light-Activated Ruthenium–Arene (RAPTA-Type) Prodrug Candidates. *ChemBioChem* **2019**, *20*, 2876–2882.

30 Riihimaki, M.; Hemminki, A.; Sundquist, J.; Hemminki, K. Patterns of Metastasis in Colon and Rectal Cancer. *Sci. Rep.* **2016**, *6*, 1–9.

TOC GRAPHIC

Patients are presenting with ever more complicated and challenging healthcare issues. Multimodal theranostic medicines are key to improving therapeutic outcomes by personalizing the treatment and imaging of cancers. A novel conjugate bearing a photosensitizing/fluorescent porphyrin tethered to a cytoactive RAPTA metal-based drug has been synthesized and investigated through *in vitro* biological evaluation.